

Exploration of the mechanism of cavitation vortex rope and vortex development in the draft tube of tubular turbine units

Chuang Cheng^{1,2}, Zhenggui Li^{1,2*}, Changrong Shen³, Shenglong Gu⁴, Chuchu Zeng⁵,
Chuanzheng Bai³, Meng Liu⁴, Junfeng Hu⁵

(1. Qinghai University of Science and Technology, Xining 810000, China;

2. Key Laboratory of Fluid and Power Machinery, Ministry of Education (Xihua University), Chengdu 610039, China;

3. South-to-North Water Diversion East Jiangsu Water Source Co., Ltd., Nanjing 210029, China;

4. School of Civil Engineering and Water Resources, Qinghai University, Xining 810016, China;

5. Dongyuan Branch of Shenzhen Water Planning and Design Institute Co., Ltd., Changsha 410000, China)

Abstract: Draft tube vortex rope is considered a special cavitation flow phenomenon in tubular turbine units. Cavitation vortex rope is one of the most detrimental factors affecting the safety of hydraulic turbines. In this study, ANSYS CFX software was utilized to numerically simulate the internal cavitation flow of a hydraulic turbine draft tube. The evolution of the cavitation vortex core was characterized by vortex line distribution and vorticity transport equation. The shape and number of blades influenced the revolving direction and distribution characteristics of the vortex close to the runner cone, which formed a counterclockwise-clockwise-counterclockwise distribution pattern. Simultaneously, there were many secondary flows in the draft tube. Mutual cancellation and dissipation between the flows was one of the reasons for reduction in vorticity. When the cross-sectional shape of the draft tube was changed, the vorticity was distributed from the center of the vortex rope to all parts of the cross-sectional draft tube, with extreme values at the center and at the walls. The vortex stretching and dilatation terms played a major role in the change in vorticity, with the baroclinic torque having an effect at the center of the vortex rope, this study is helpful to understand the flow of water in the draft tube and guide the design and optimization of the draft tube in engineering application.

Keywords: cavitation, vortex rope, vorticity transport equation, vortex line, draft tube

DOI: [10.25165/j.ijabe.20241701.8143](https://doi.org/10.25165/j.ijabe.20241701.8143)

Citation: Cheng C, Li Z G, Shen C R, Gu S L, Zeng C C, Bai C Z, et al. Exploration of the mechanism of cavitation vortex rope and vortex development in the draft tube of tubular turbine units. *Int J Agric & Biol Eng*, 2024; 17(1): 163–171.

1 Introduction

Bulb-tubular turbine units are among the most important models for the development of low-head hydraulic resources^[1]. They are runoff-regulating units whose operating conditions are often influenced by upstream incoming flow^[2,3]. These units have a significant impact on cavitation performance of overflow components during conditions transformation or operational scheduling^[4,5], especially in draft tubes, where cavitation vortex ropes tend to form^[6]. The flow state and field characteristics in draft tubes change with the shape of the cavitation vortex rope. The core of the cavitation vortex rope is the vortex zone, which mainly affects the efficiency of and destroys the material on the surface of hydraulic turbines^[7], causing rotating cavitation stalls and turbulence. To address the generation and development of tailwater

vortex ropes in tubular hydraulic turbines, Peng et al.^[8] analyzed the flow characteristics of a tailwater vortex rope for small and large flow rates of the unit based on regularized helicity, flow line analysis vortex, and vortex rope. He found that partial working conditions lead to unit instability owing to the spiral vortex rope. Kim et al.^[9] captured inter-blade vorticity development of a tail water vortex rope inside a runner channel at low flow rates. Although the vortex rope development was not apparent inside the draft tube under high-intensity cyclonic flow and a low flow rate, the high vorticity made the vortex rope flow very complex and created a wide range of backflows inside the draft tube. The development of inter-leaf and tailwater rope vortices depends on the flow and velocity characteristics of the rotor inlet and outlet. Ji et al.^[10] used a scale-adaptive simulation method and a diffuser with cyclonic flow to simplify and simulate the non-contact flow inside a draft tube to reveal the potential mechanism between the structure of the vortex rope and the cavitation vortex. From the analysis of the vorticity transport equation, it was concluded that the vorticity expansion term is larger along the cavity interface and the vorticity field is modified in the region of higher density and pressure gradients.

The cavitation method followed by the vortex development study has been used to investigate the interaction between cavitation and vortices. Podnar et al.^[11] studied the effect of hydrofoil shape on the blade flow characteristics of a bulb-tubular hydraulic turbine. The flow on the suction side of the hydrofoil in the cavitation channel was visually studied to avoid flow separation and vortex generation. He improved the blade airfoil shape by increasing the

Received date: 2023-01-12 Accepted date: 2023-10-19

Biographies: Chuang Cheng, MS candidate, research interest: fluid machinery, Email: 492668808@qq.com; Changrong Shen, Senior Engineer, research interest: hydraulic engineering, Email: 2213491305@qq.com; Shenglong Gu, Professor, research interest: computational hydraulics, Email: sl.gu@qhu.edu.cn; Chuchu Zeng, Assistant Engineer, research interest: hydraulic engineering, Email: 1729728965@qq.com; Chuanzheng Bai, Senior Engineer, research interest: water resources construction and management, Email: 13527420165@163.com; Meng Liu, Tutor, research interest: computational hydraulics, Email: liumn@qhu.edu.cn; Junfeng Hu, Engineer, research interest: hydraulic engineering, Email: 909485788@qq.com.

*Corresponding author: Zhenggui Li, Professor, research interest: fluid machinery. Xihua University, Chengdu 610039, China. Tel: +86-17602832345, Email: lzhgui@mail.xhu.edu.cn.

leading-edge radius, maximum thickness, and curvature to stabilize the flow around the hydrofoil towards the trailing edge. In an effort to gain a comprehensive understanding of cavitation-vortex interaction, Huang et al.^[12] argued that the development of cavitation increases the vorticity generation and flow instability in mixed-flow jet pumps. Vortices are located at the cavity interface during cavitation. The analysis using the relative vorticity transport equation shows a steep increase in vortex dilatation and baroclinic torque when cavitation occurs, particularly at the downstream interface. However, vortex dilatation is the fundamental cause of large-scale vortex generation. Sun et al.^[13] conducted a study on cavitation vortices between blades of a mixed-flow model hydraulic turbine. The results showed that the interblade cavitation vortex structure is characterized by a spiral twist and attachment to the hub of the rotor, extending to the exit of the rotor. At the same time, the vorticity transport equation details the terms that play a dominant role in the vortex development process and improves the knowledge of vortex dynamic characteristics and formation. Sun et al.^[14] also identified and studied tailwater vortex rope morphology using different vortex analysis methods for a mixed-flow hydraulic turbine. They concluded that the isobaric method was incapable of capturing vortex rope morphology. The Ω method has a somewhat dimensionless but over-predicted tail morphology, whereas the recently developed Liutex method is comparable to the Q criterion and λ_2 . They both show the morphology of the vortex rope as it rotates.

In summary, the development of a cavitation vortex rope and the formation and distribution of the vortex structure within the draft tube are critical issues in the study of the flow regime within a hydraulic turbine. This has a bearing on draft tube energy recovery and vibration stability. Viscous forces exist in both the draft tube wall and water flow, and the water body has poor shear resistance. Therefore, there was a large velocity gradient from the middle of the draft tube to the wall. After the rotation of the runner, the fluid microclusters rotated along the runner cone. The draft tube was designed with a progressively larger cross-section, resulting in violent vortex movements, partial reflux, and energy loss within the draft tube. To investigate the effect of cavitation on tailwater vortex rope motion and vortex evolution, numerical simulations of gas-liquid two-phase flow at critical cavitation (cavitation coefficient is $\sigma_p = 1.781$) were conducted in this study, aiming to illustrate the cavitation vortex rope and the corresponding vortex structure of the draft tube. The formation and development of these structures were simultaneously investigated, using the vorticity transport equation to analyze the vortex structure and summarize its motion and distribution laws.

2 Computational model and meshing

2.1 Control equations and turbulence model

The shear stress transport (SST) $k-\omega$ turbulence model was used. In addition to the ability to transport shear stresses, the sidewall viscosity was also considered^[15]. The Zwart-Gerber-Belamri model was chosen as the cavitation model. The model is based on the simplified Rayleigh-Plesset equation, which is well coupled to various turbulence equations and has high prediction accuracy. The expression for the SST $k-\omega$ model is given below^[16,17]:

$$\frac{\partial(\rho k)}{\partial t} + \frac{\partial(\rho u_i k)}{\partial x_i} = \tilde{P}_k - \beta^* \rho k \omega + \frac{\partial}{\partial x_i} \left[(\mu + \sigma_k \mu_i) \frac{\partial k}{\partial x_i} \right] \quad (1)$$

$$\frac{\partial(\rho \omega)}{\partial t} + \frac{\partial(\rho u_i \omega)}{\partial x_i} = \alpha \rho S^2 - \beta^* \rho \omega^2 + \frac{\partial}{\partial x_i} \left[(\mu + \sigma_\omega \mu_i) \frac{\partial \omega}{\partial x_i} \right] - 2(1 - F_1) \rho \sigma_{\omega 2} \frac{1}{\omega} \frac{\partial k}{\partial x_i} \frac{\partial \omega}{\partial x_i} \quad (2)$$

where, \tilde{P}_k is the amplitude-limiting term; F_1 is the mixing function; α , β^* , σ_k and $\sigma_{\omega 2}$ are model constants.

The net mass transfer rate of the vacuole in the ZGB model is expressed as follows:

$$\begin{cases} R_c = F_{\text{vap}} \frac{3\alpha_{\text{nuc}}(1 - \alpha_v)\rho_v}{R_B} \sqrt{\frac{2}{3} \frac{P_v - P}{\rho_l}}, & P < P_v \\ R_c = F_{\text{cond}} \frac{3\alpha_v \rho_v}{R_B} \sqrt{\frac{2}{3} \frac{P - P_v}{\rho_l}}, & P > P_v \end{cases} \quad (3)$$

where, α_{nuc} is the volume fraction of the gas core, which is usually assumed to be 5×10^{-4} . F_{vap} is the evaporation coefficient, which is often taken as 50. P_v is the saturated vapor pressure. F_{cond} is the condensation experience factor, which was set as 0.01.

In fluid mechanics, the unique expression of the law of conservation of mass is the continuity equation^[18]. Assuming that the gas and liquid phases share the same pressure and velocity fields, the control equation is as follows:

$$\frac{\partial \rho}{\partial t} + \nabla(\rho \vec{v}) = 0 \quad (4)$$

$$\frac{\partial}{\partial t} (\rho \vec{v}) + \nabla(\rho \vec{v} \vec{v}) = -\nabla p + \nabla \left(\mu \left[(\nabla \vec{v} + \nabla \vec{v}^T) - \frac{2}{3} \nabla \vec{v} I \right] \right) + \rho \vec{g} + \vec{F} \quad (5)$$

where, ρ is the fluid density; \vec{v} is the velocity vector; p is the static pressure; $\rho \vec{g}$ and \vec{F} are gravitational and external forces, respectively; μ is the dynamic viscosity, and I is the unit tensor. The volume fraction α_m and density ρ_m of the mixed phase are as follows:

$$\alpha_m = \alpha_l + \alpha_v \quad (6)$$

$$\rho_m = 1 / \left(\frac{y_v}{\rho_v} + \frac{y_l}{\rho_l} \right) \quad (7)$$

where, α_l and α_v are the liquid and gas phase volume fractions, respectively; y_l and y_v are the liquid- and gas-phase mass fractions, respectively. Simultaneously, the mass fraction y satisfies the following:

$$y_l + y_v = 1 \quad (8)$$

2.2 Tubular hydraulic turbine model and meshing

The tubular hydraulic turbine model was numerically simulated using a 1:1 sized real machine. The model has 4 rotor blades and 16 guide vanes, of which specific parameters are listed in Table 1.

Table 1 Technical parameters of tubular turbine units

Parameter name	Parameter value
Rotor diameter	7.27 m
Synchronous speed	68.18 r/min
Rated output of single machine	26.8 MW
Rated flow rate	378 m ³ /s
Highest head	12 m
Minimum head	2.6 m
Rated head	6.8 m
Number of blades	4
Number of guide vanes	16

The unit studied has an inlet flow of 270.781 m³/s, head of 8.24 m, paddle opening of 25° and guide vane opening of 54.8° for the combined operating conditions^[19]. The overall model is divided into five sections: the inlet section, bulb body, guide vane, runner, and draft tube, as illustrated in Figure 1 above. Owing to the complex structure of the guide vane and runner sections, a

tetrahedral mesh was used^[20]. For the cavitation calculation, the number of grid cells has a large impact on the hydraulic turbine cavitation characteristics^[21]. To reduce the influence of the grid number on the calculation accuracy, the correspondence between the overall grid number of the hydraulic turbine, the cavitation coefficient of the hydraulic turbine, and the minimum pressure of the vortex rope of the draft tube under combined working conditions was analyzed, as shown in Figure 2. As the number of grid nodes increased, the minimum pressure of the draft tube vortex rope of the hydraulic turbine decreased. When the number of grids reached 6 million or more, the cavitation coefficient changed slightly. When the number of grids exceeded 8 million, the minimum pressure of the draft tube reached its lowest point. Therefore, a grid of 8.84 million was chosen as the initial grid for the calculation.

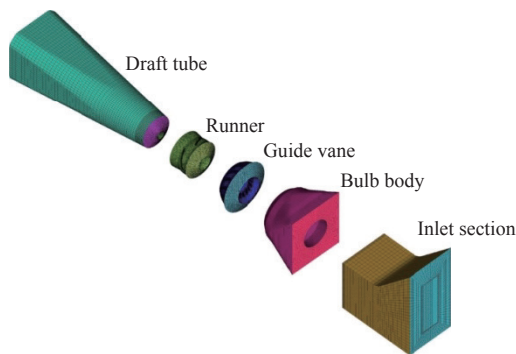


Figure 1 Components and meshing of the fluid domain of the tubular hydraulic turbine

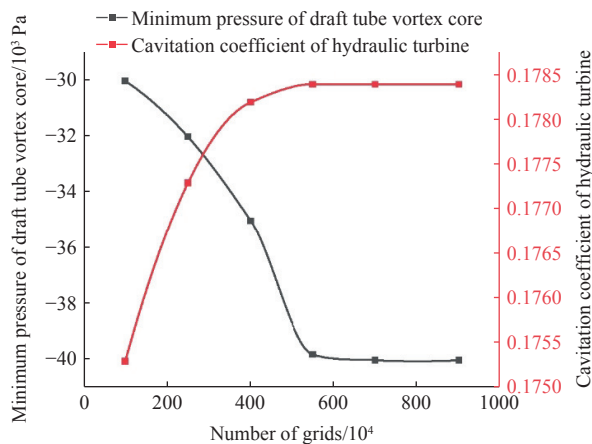


Figure 2 Grid-independent verification

2.3 Numerical simulation method and boundary conditions

In the 25.0°-54.8° combined working conditions, the mass flow inlet (bulk mass flow rate) was selected for the inlet section, and the pressure outlet (opening pressure and Dirn) was selected for the draft tube outlet. A no-slip wall was used for all walls, and the speed was set at 68.18 r/min. The cross interface was selected from the frozen rotor for steady-state simulation and the transient rotor-stator for transient simulation. It selects the high-accuracy solution mode and the steady-state calculation results as the initial condition for cavitation. The transient calculation was set to one step every 3°, which was 0.007 335 s. Sixteen revolutions were performed, and the last one was selected as the result. Critical cavitation is considered to occur when the efficiency of a hydraulic turbine decreases by 1%. Here, the cavitation pressure is the critical cavitation pressure^[22].

The hydraulic turbine critical cavitation pressure coefficient is defined as follows:

$$\sigma_p = \frac{\frac{P_0}{\rho g} - \frac{P_c}{\rho g} - H_s}{H} \quad (9)$$

where, P_0 is the draft tube outlet pressure; P_c is the saturation vapor pressure of water; ρ is the density of water; g is the acceleration of gravity; H_s is the hydraulic turbine suction height; H is the working head of the hydraulic turbine. The critical cavitation pressure is obtained by varying the outlet pressure of the draft tube. The critical cavitation coefficient $\sigma_p = 1.781$ can be determined for this co-located condition, as shown in Figure 3.

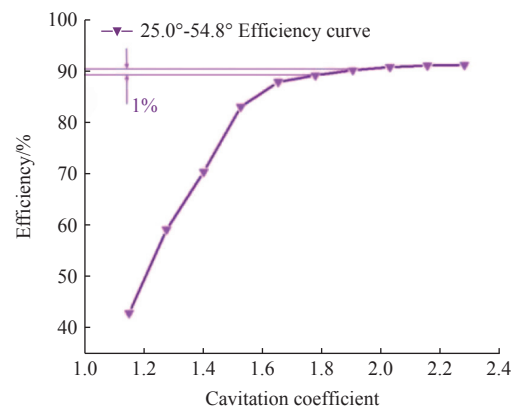


Figure 3 Cavitation coefficient and efficiency curve

3 Experimental verification of external characteristics

The pressure pulsations caused by the evolution and development of the draft tube vortex rope of the bulb tubular turbine units can affect the main shaft due to unbalanced hydraulic forces, causing it to vibrate. To verify the reliability of the CFD numerical simulation results, the tubular turbine units were tested for shaft vibration and tailwater pressure pulsation under the same co-location conditions. An EJA530E pressure transmitter was used for digital signal acquisition of the pressure inside the flow field. Simultaneously, the hair guide bearing +X, +Y oscillation, combination bearing +X, +Y oscillation, water guide bearing +X, +Y oscillation, engine guide bearing +X, +Y, +Z vibration, combination bearing +X, +Y, +Z vibration, water guide bearing +X, +Y, +Z vibration, bulb body +X, +Y, +Z vibration, and runner room +X, +Y, +Z vibration were used to monitor specific vibration and oscillation measurement points as shown in Figure 4.

Pressure pulsation monitoring was performed under critical cavitation conditions. Figure 5 shows a comparison between the test and calculated results at the center of the draft tube pressure monitoring section. The red dotted line and the black curve represent the test and calculated values, respectively. It can be observed that the numerically calculated values follow the same trend as the experimental results and are aligned, indicating that the numerically calculated results are reliable.

Cavitation worsens the pressure pulsations and vibrations inside the hydraulic turbine, affecting the stability of the hydraulic turbine^[23,24]. In Figure 6, the black and blue curves correspond to the frequency domain diagrams obtained by the fast Fourier transform (FFT) of the pressure pulsations at the center of the monitored sections under no cavitation and cavitation conditions, respectively.

The four monitoring sections were 17 m, 22 m, 34 m, and 47 m from the center of the rotor. It can be established that the main frequency in the cavitation condition is 1 fn (fn is the rotational

frequency), which is the frequency of the vortex rope formed by the cavitation. The cavitation vortex rope formed extends downstream, with the pulsation value decreasing in the direction of the flow.

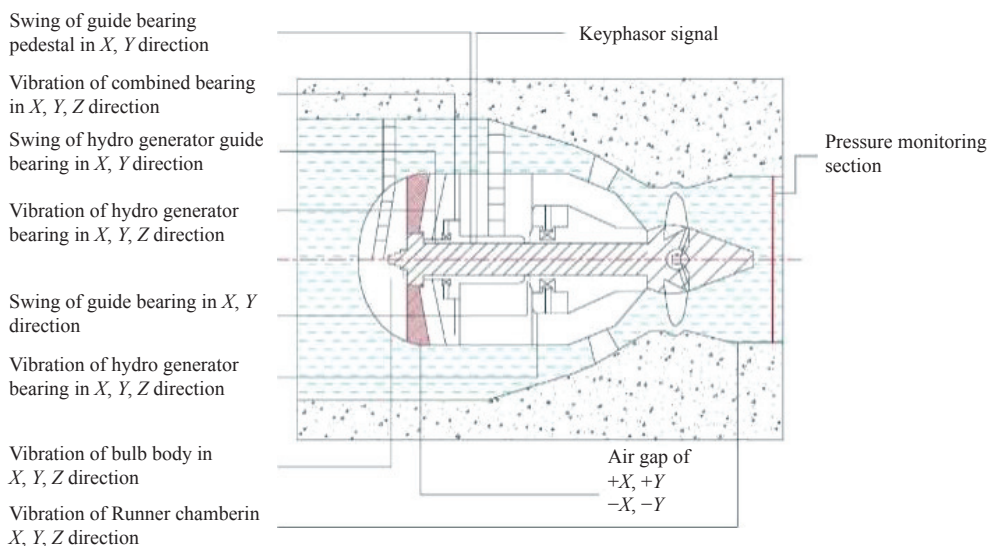


Figure 4 Location of vibration and oscillation measurement points

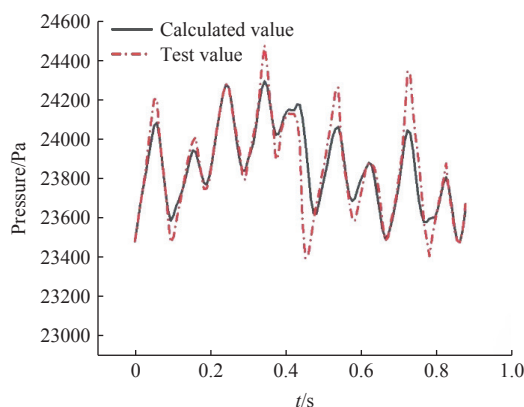
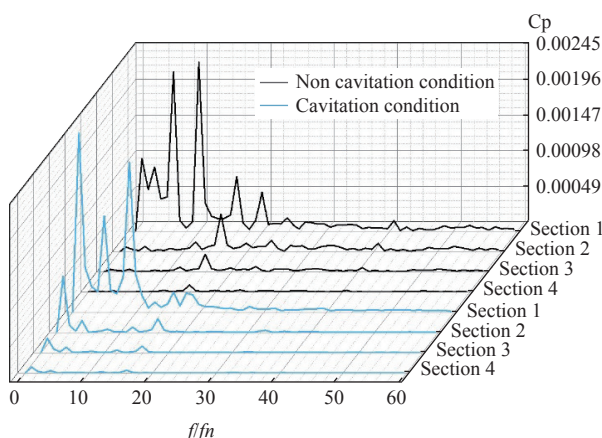


Figure 5 Calculated and experimental values of the central pressure in the draft tube



Note: C_p is the pressure pulsation amplitude, $C_p = (P - P_{ave}) / \rho g H$, P is the pressure, P_{ave} is the average value of P , ρ is the density of water, and H is the working head.

Figure 6 Cavitation and non-cavitation conditions pressure pulsation frequency domain diagram

Figure 7 shows the results of the four active power water guide-bearing vibration tests under this condition. The magnitude of the vibration (μm) in the x -direction (axial direction) is shown in the graph. It can be observed that the maximum amplitude occurs at

1 fn, at the tailwater vortex rope frequency. This indicates that the vibration of the water guide bearing was mainly influenced by the turbulence of the tailwater vortex rope. This is followed by 4 fn, where the vibration is caused by pressure pulsations caused by the rotation of the runner. In addition, some small peaks are caused mainly by mechanical factors and unstable magnetic tension between the stator and the rotor. The test results prove that the vortex frequency caused by cavitation in the draft tube is the main factor causing the vibration of water-guided bearings.

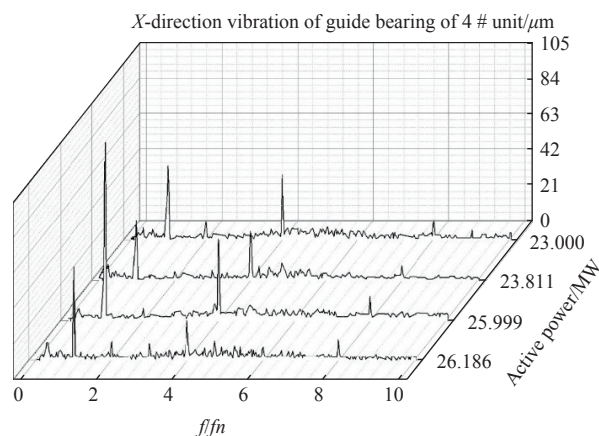


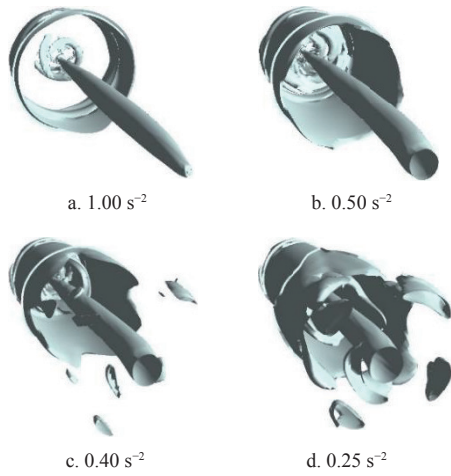
Figure 7 Vibration test of water-guided bearing under critical cavitation condition

4 Analysis of numerical simulation results

4.1 Distribution and development of cavitation vortex rope and vortex of the draft tube

As observed from the vortex rope equivalent surface of the draft tube in Figure 8, there are four small vortex ropes rotating around the central vortex rope. This is owing to the amount of ring that forms at the draft tube inlet after passing the water exit edge of each rotor blade and rotating in the axial and circumferential directions, and its subsequent gradual disappearance during movement. The central vortex rope was distributed in a straight line in the direction of the water flow and gradually increased in

diameter. A gradual change in the cross-sectional shape of the draft tube can be clearly observed as a result of the cross-sectional change, resulting in a more dispersed vorticity distribution. The vorticity values gradually decreased in the flow direction, resulting in a more dispersed vorticity close to the draft tube outlet.



Note: s^{-2} is the unit of the vortex rope equivalence surface.

Figure 8 Vortex rope equivalence surface of draft tube

Figure 9 shows the pressure distribution in the meridional plane of the tubular turbine units and the draft tube cross-sectional setup. The cavitation vortex rope within the draft tube is centrally located, which is a similar position as the central vortex rope distribution in Figure 8. To investigate the development of the tailwater vortex cavitation vortex rope, four cross-sections were set up in the draft tube. The draft tube cross-section was set at the exit of the runner cone (cross-Section 1), development surface of the cavitation vortex rope (cross-Section 2), tapering surface of the draft tube shape (cross-Section 3), and cross-section close to the draft tube exit

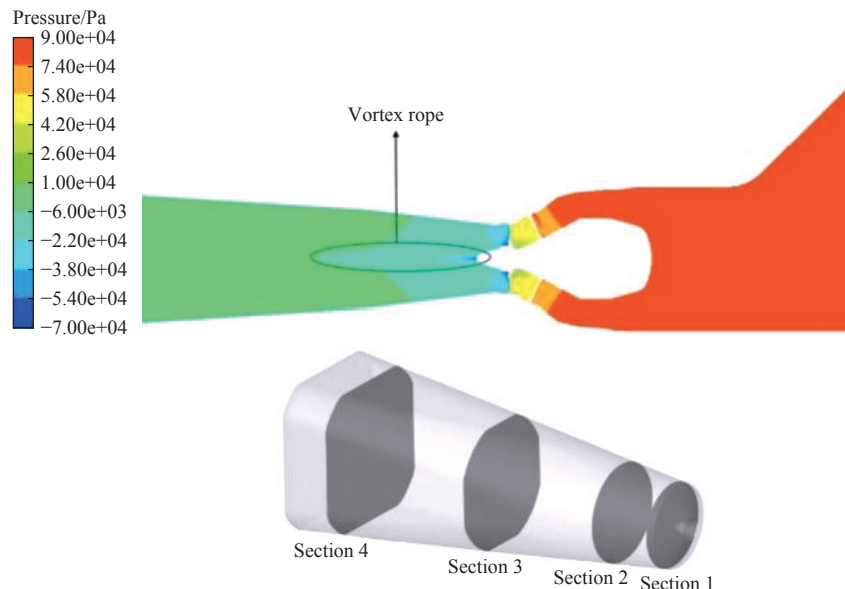


Figure 9 Pressure distribution in the meridional plane and cross-sectional setup of the draft tube

As illustrated in Figure 10b, the Q criterion maximum remained at the vortex core position of the cavitation vortex rope, the vortex core area increased, and the direction of rotation remained the same. Simultaneously, there was a clockwise rotating horseshoe vortex close to the vortex core. This is due to the low pressure close to the cavitation vortex core and the high pressure away from the core. As

(cross-Section 4). These four sections allowed the flow pattern to be determined at different locations as the water passed through.

The concept of a vortex line refers to a curve along which the tangent line at any given point aligns with the vorticity vector of the fluid at that particular point, while also being tangential to the vorticity field throughout a specific moment in time. The four cross-sectional vortex distributions were analyzed to investigate vortex distribution and development in the draft tube. Figure 10 shows the cross-sectional Q-criterion with a vortex line distribution, where the vortices rotating clockwise and counterclockwise are indicated in purple and yellow, respectively. Thirteen vortices of different sizes and orientations are clearly observed in Figure 10a. The Q-criterion maximum occurred in the middle of the section, where the vortex line was clustered with the largest vorticity value and the vortex direction was counterclockwise. This is consistent with the previous analysis, which showed four clockwise vortices of the same shape along the increasing radius. This is due to the fact that the blade width at the rim of the tubular turbine units is greater than the blade width at the hub and the spatially distorted shape of the blades at the water's exit. The velocity of the water flow has a certain component in the circumferential direction after the work has been completed. Therefore, the velocity at the edge of the shroud is greater than that at the hub. Owing to viscosity, a velocity difference was created at the outlet edge, resulting in a clockwise vortex, which was then deflected by the runner cone to create four clockwise vortices with the same number of blades in the draft tube. Four counterclockwise rotating vortices with accompanying small vortices attached to them in the opposite rotating direction can be found close to the draft tube wall, and the velocity gradient was large in this area. As a result, the small vortices are elliptical in shape due to the shear. There was no independent vortex movement close to the wall. Overall, the vortex pattern from the center of the draft tube to the wall was mainly counterclockwise-clockwise-counterclockwise.

a result of the pressure gradient, the vortex moved closer to the vortex core, thus creating a horseshoe vortex around the cavitation vortex core. As can be seen in the diagram, the horseshoe vortex at this point was a fusion of the two clockwise vortices outside the vortex core in Section 1. It is evident that the other two clockwise rotating vortices dissipated and disappeared. In addition, the two

counterclockwise vortices close to the wall area fused gradually. It is clear that in Section 2, adjacent vortices with opposite directions of rotation dissipated and cancelled each other out, and that some of the vortices were fused and regrouped to form new vortices.

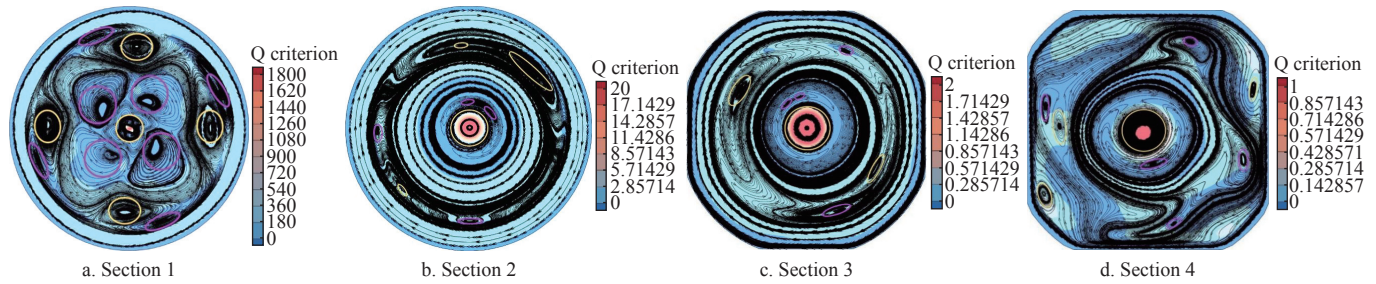


Figure 10 Q-criterion with vortex line distribution for each section under critical cavitation conditions

The two counterclockwise vortices in Section 2 were fused into one as the draft tube rotated counterclockwise, as shown in Figure 10c. Simultaneously, the distance between the two vortex cores inside the horseshoe vortex gradually decreased and merged. The two counter-rotating vortices were close to each other by the wall. Owing to the different directions of rotation and deformation under shear, the vortex shape flattened, and the number of vortices was reduced from eight to seven.

In Figure 10d, the two clockwise rotating vortices at the center of the horseshoe vortex merged into one. Simultaneously, the number of vortices increased across the cross section. Most of the vortices at this point were concentrated near the wall of the draft tube. In practice, when holistically viewed, it is easy to observe that the vortices are affected by viscous forces as well as some of the small backflows as they move downstream. They all moved away from the center of the vortex core, gradually getting closer to the draft tube wall. On the one hand, the viscous effect is more pronounced near the solid wall. On the other hand, the flow velocity decreased because of the increased cross-sectional area and the change in the shape of the draft tube. The flow in a square section would likely generate velocity more differences and form vortices than that in a circular section. Therefore, the vortices tend to be concentrated near the walls of the draft tube.

The degree of cavitation was more severe near the runner cone. Owing to the influence of the cavitation vortex core, the draft tube had a higher pressure than the central vortex core. Consequently, there was a large pressure gradient, and the flow near the vortex core formed a horseshoe vortex. The distribution of the vortex line in these four cross-sections is a good indication that the flow inside the draft tube generates a particularly high number of secondary flows and that these flows with different rotational directions cancel and consume each other. Moreover, the increase in the cross-sectional area and the change in the shape of the draft tube led to an increased viscous dissipation of the flow energy. This explains the gradual decrease in the vorticity of the flow in the draft tube. The flow became progressively messier from a regular counterclockwise-clockwise-counterclockwise distribution in Section 1. In Section 4, vortices with different rotational directions approach the solid side walls.

4.2 Analysis of the formation mechanism of cavitation vortex rope in draft tube

The vortex rope inside the draft tube of tubular turbine units is another cavitation phenomenon. The causes are also more complex. In general, many different factors can lead to the formation of cavitation vortex ropes. To determine the influence of different factors on the cavitation vortex rope and vortex distribution, the

Consequently, the number of vortices was reduced from 13 to 8. The vortices in cross-Section 1 were evenly distributed, whereas in cross-Section 2, they were mostly concentrated in the middle of the radius.

vorticity transport equation is introduced to describe the causes of vortex rope formation. By performing a spin calculation on the Navier–Stokes equation, the vorticity transport equation for a viscous compressible fluid can be obtained as follows^[25]:

$$\frac{d\omega}{dt} = (\omega \nabla) V - \omega (\nabla V) + \nabla f - \nabla \left(\frac{1}{\rho} \right) \nabla P + \nu \nabla^2 \omega \quad (10)$$

where, ω represents vorticity, s^{-2} . V is the combined velocity, m/s. f represents the non-conservative force; ρ is the density of the water-gas mixture, kg/m^3 . P is the pressure, Pa. ν denotes viscosity, Pa·s. The rate of change of vorticity against flow time is on the left-hand side of Equation (7), with the first term on the right-hand side, $(\omega \nabla) V$ representing the stretching and bending of the vortex line due to the velocity gradient of the flow field. This change results in a change in the size and direction of the vorticity:

$$(\omega \nabla) V = \left(\omega_x \frac{\partial V_x}{\partial x} + \omega_y \frac{\partial V_x}{\partial y} + \omega_z \frac{\partial V_x}{\partial z} \right) i + \left(\omega_x \frac{\partial V_y}{\partial x} + \omega_y \frac{\partial V_y}{\partial y} + \omega_z \frac{\partial V_y}{\partial z} \right) j + \left(\omega_x \frac{\partial V_z}{\partial x} + \omega_y \frac{\partial V_z}{\partial y} + \omega_z \frac{\partial V_z}{\partial z} \right) k \quad (11)$$

The second term $\omega (\nabla V)$ on the right hand side represents the change in size of the vorticity caused by the change in volume of the fluid micro-cluster. A contraction in the volume of the fluid mass increases vorticity and vice versa:

$$\omega (\nabla V) = \left(\omega_x \frac{\partial V_x}{\partial x} + \omega_x \frac{\partial V_y}{\partial y} + \omega_x \frac{\partial V_z}{\partial z} \right) i + \left(\omega_y \frac{\partial V_x}{\partial x} + \omega_y \frac{\partial V_y}{\partial y} + \omega_y \frac{\partial V_z}{\partial z} \right) j + \left(\omega_z \frac{\partial V_x}{\partial x} + \omega_z \frac{\partial V_y}{\partial y} + \omega_z \frac{\partial V_z}{\partial z} \right) k \quad (12)$$

The third term ∇f on the right hand side is the contribution of the body force. In general, only non-conservative forces can cause a change in vorticity. In the rotating reference system, the Coriolis force is negligible for the draft tube. The fourth term on the right hand side is the baroclinic torque induced by the density gradient. For positive pressure fluids, this term is 0. For diametrically pressurized fluids alone, thermal convection is generated, which causes a change in vorticity:

$$\left(\nabla \frac{1}{\rho} \nabla P \right) = \left(\frac{\partial}{\partial y} \frac{1}{\rho_y} \frac{\partial P_z}{\partial z} - \frac{\partial}{\partial z} \frac{1}{\rho_z} \frac{\partial P_y}{\partial y} \right) i + \left(\frac{\partial}{\partial z} \frac{1}{\rho_z} \frac{\partial P_x}{\partial x} - \frac{\partial}{\partial x} \frac{1}{\rho_x} \frac{\partial P_z}{\partial z} \right) j + \left(\frac{\partial}{\partial x} \frac{1}{\rho_x} \frac{\partial P_y}{\partial y} - \frac{\partial}{\partial y} \frac{1}{\rho_y} \frac{\partial P_x}{\partial x} \right) k \quad (13)$$

The fifth term on the right hand side, $\nu \nabla^2 \omega$ represents the vorticity viscous diffusion effect. In flows with high Reynolds

number, this viscous diffusion term is negligible^[13]. Figures 11-14 depict the distribution of the vortex stretching, vortex dilatation, and

baroclinic torque terms in the vorticity transport equation for the four cross sections.

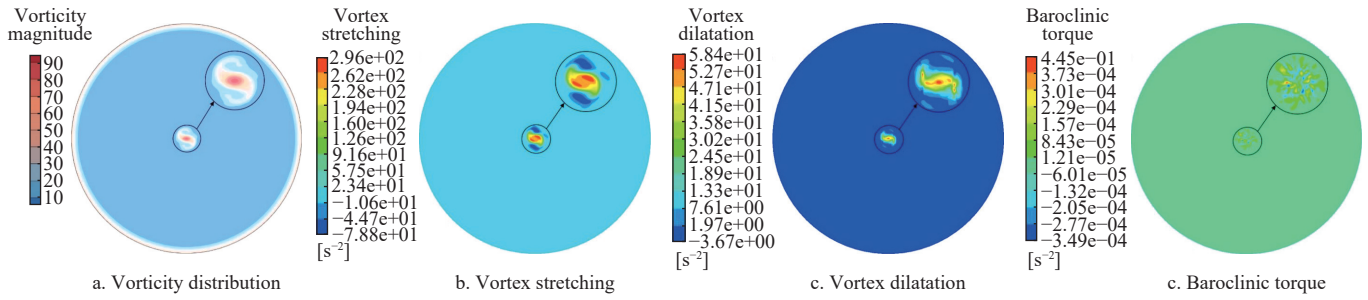


Figure 11 Vorticity distribution, vortex stretching, vortex dilatation, and baroclinic torque terms of Section 1

Figure 11a shows vorticity distribution in draft tube Section 1. The center of the vortex core is where vorticity accumulates and reaches a peak with a maximum value of approximately 92 s^{-2} . The vorticity gradient varies sharply in the direction of the increasing radius. The runner cone brings together a strong cyclonic flow that passes through the blades. The vorticity is therefore very concentrated here, and the maximum vorticity values are located in the center of the vortex core. The vorticity close to the wall is caused by the shear motion and is not described later. The vortex stretching term is shown in Figure 11b, where the distribution of this component is almost identical to that of vorticity. The red region in the center of the tailwater vortex core is where the absolute value of vortex stretching is the greatest. This is also the most important factor in the variation in vorticity in this section. The vortex dilatation term also affects vorticity variation, as shown in Figure 11c. It can be observed that the stretching and expansion terms occur simultaneously. As it is at the center of the cavitation vortex core, the volume contraction at this point causes a change in rotational inertia, which in turn triggers a change in vorticity. The expansion term is an order of magnitude lower than the stretching term. However, the effect of this term is significant. In cavitation flow, vacuoles and currents induce changes in density, as well as inhomogeneous pressure distribution. Therefore, the baroclinic torque term is not negligible, as shown in Figure 11d. This term is more apparent in the center of the cavitation vortex core in the draft

tube. In Section 1, the vortex stretching term is the main factor affecting the change in vorticity. Thus, the vorticity distribution (a) and vortex stretching (b) distribution ranges were essentially the same.

Figure 12a shows the vorticity distribution for Section 2, with a maximum vorticity of approximately 14 s^{-2} at the center of the cavitation vortex core and a uniform distribution of vorticity along a gradient. Figure 12b shows the vortex stretching term. It can be seen that the red area is where the term is smallest, and the blue area is where it is largest in absolute terms. Therefore, for cross-Section 2, the vortex stretching term acts mainly at the location of the cavitation vortex core. The blue area had a horseshoe shape at the center of the vortex core. This may also be one reason for the horseshoe vortex in the vortex line diagram. The vortex dilatation term is shown in Figure 12c; this term is also concentrated in the center of the vortex core and is centrosymmetrically distributed. Apart from the outer ring, the interior was dominated by eight bands of expansion terms of almost equal absolute magnitudes. The distribution of the baroclinic torque is shown in Figure 12d, where the distribution of the baroclinic torque is still concentrated in the vortex core. Compared with the other two terms, this term had a smaller effect on vorticity. The absolute value of the vortex dilatation term was larger than that of the stretching term. However, the area of the stretched part was actually larger than that of the expanded part; therefore, Section 2 was still dominated by the stretching term.

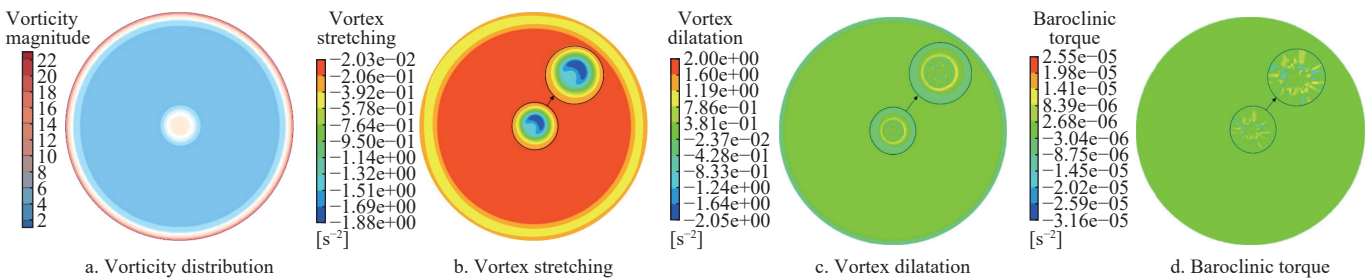


Figure 12 Vorticity distribution, vortex stretching, vortex dilatation, and baroclinic torque terms of Section 2

In Figure 13a, it can be seen that the maximum value of the vortex core vorticity center is only 6 s^{-2} at Section 3, and there is a partial inverse vorticity gradient. Compared to the first two sections, the distribution of vortex stretching terms in Section 3 was more dispersed. Except for the vortex core, the largest absolute values were concentrated near the solid wall of the draft tube. This phenomenon is caused by the transition from a circular to a square draft tube section, which results in a large flow velocity gradient at the wall surface. In addition, the inverse vorticity gradient is

partially caused by the vortex stretching term. The vortex dilatation term increased in the center of the vortex rope of the draft tube compared to Section 2, which was also partially present near the side walls of the draft tube. The baroclinic torque term was distributed throughout this section but remained more concentrated in the center of the cavitation vortex core. In terms of numerical magnitude, the baroclinic torque had less influence on the vorticity distribution.

In Section 4, the vortex core center vorticity was only 3 s^{-2} at its

maximum, with a very small vorticity gradient. As shown in the vorticity diagram, the vortex core had the largest central vorticity distribution. As described in Section 3, it still had an inverse vorticity gradient. The vortex stretching term continued to show extremes at the solid wall boundaries in addition to the center of the vortex core and was concentrated at the boundary shape changes.

The inverse vorticity gradient was mainly caused by the stretching term. The range of the distribution of the vortex dilatation term increased as the vortex core range increased. As with the stretching term, extreme values occurred at the boundary shape change. The baroclinic torque term was mainly distributed at the center of the vortex core and has less influence on the vorticity distribution.

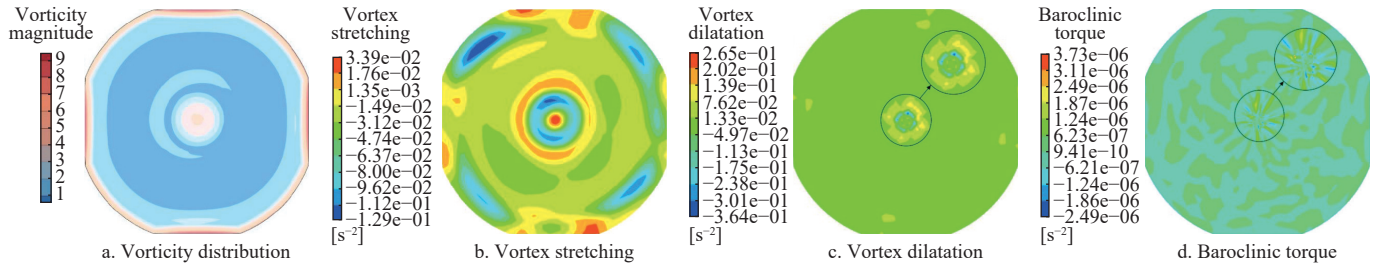


Figure 13 Vorticity distribution, vortex stretching, vortex dilatation, and baroclinic torque terms of Section 3

Overall, the vorticity was depleted by viscous forces as the water moved towards the draft tube outlet. It can be easily observed from the change in vorticity size that the vorticity distribution, vortex stretching, vortex dilatation, and baroclinic torque terms all decreased gradually from Sections 1 to 4, with significant viscous dissipation of the water flow. At the same time, the vorticity inside the draft tube was larger, especially in the center of the vortex core. The change in vorticity owing to the baroclinic torque was smaller. Before the change in the draft tube cross-sectional shape, all the factors influencing the change in vorticity were located at the center of the vortex core of the vortex rope of the draft tube. After the change in the cross-sectional shape, the tensile and expansion terms arose at the wall shape gradient and were more widely distributed.

each component of the vorticity transport equation at four sections, as illustrated in Figure 15, the overall observation indicates that as the cross-sections move farther away from the center of the turbine runner, vortices gradually dissipate, and vorticity diminishes. This trend is also reflected in the three components of the equation. Throughout the entire cross-section near the turbine runner (cross-Sections 1 and 2), all components exhibit a continuous decrease, with the vortex dilatation term being the primary contributor to vorticity variations. However, as we move closer to the draft tube outlet (cross-Sections 2 and 3), the rate of decrease in the vortex dilatation term lessens, while the vortex stretching term and the baroclinic torque term gradually increase. This observation suggests that, near the draft tube outlet, vortices undergo stretching, resulting in an expansion of their volume and an increase in their length as they move downstream.

To provide a more intuitive representation of the distribution of

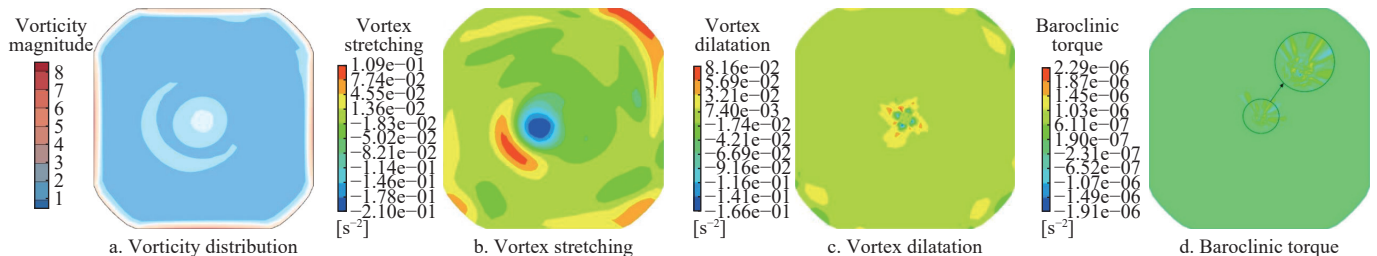


Figure 14 Vorticity distribution, vortex stretching, vortex dilatation, and baroclinic torque terms of Section 4

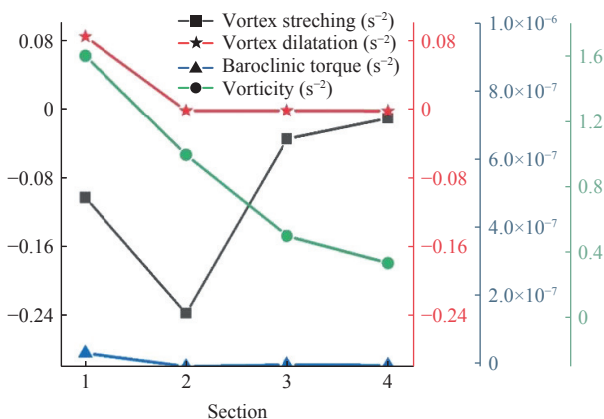


Figure 15 The average distribution of the factors of the equation in four cross sections

5 Conclusions

In this study, numerical simulations were used to investigate

the development of cavitation vortex rope and flow, the development characteristics of the draft tube of the tubular hydraulic turbine group, and the distribution range and mode of action of the three factors causing vorticity changes.

The results of the study show that the cavitation vortex rope of the draft tube is distributed in a straight line in the flow direction, with a gradual increase in the cross-sectional area along the diameter during development. The shape and number of blades influence the revolving direction and distribution characteristics of the vortex close to the runner cone, forming a counterclockwise–clockwise–counterclockwise distribution pattern in the direction of radius increase. However, owing to viscous forces, the vortex gradually moves closer to the solid sidewalls as it develops in the draft tube, gradually breaking this distribution pattern. Pressure changes from horseshoe vortices inside the draft tube as a result of cavitation. At the same time, there are many secondary flows in the draft tube, canceling out and dissipating each other, causing the reduction in vorticity. The vortex stretching and dilatation terms

play a major role in the change in the vorticity of the tailwater vortex rope. The vortex stretching, vortex dilatation, and baroclinic torque terms are mainly concentrated at the vortex rope and core before the change in the cross-sectional shape of the draft tube. After the change in the draft tube cross-sectional shape, these terms were distributed throughout the draft tube cross-section, with extreme values occurring at the center of the vortex core and near the wall. The inverse vorticity gradient in the draft tube was mainly caused by the vortex stretching term.

The study of the cavitation vortex rope and vortex distribution in draft tubes helps to systematically illustrate the relationship between cavitation and the flow pattern in draft tubes and vortex formation. The shape of the draft tube in tubular turbine units is not complex; therefore, this study is useful as a reference for the adaptation, hydraulic optimization, and design of draft tubes.

This study mainly focus on the mechanism of cavitation vortex rope in draft tube, it lacks a consensus result on the vortex rope formed in the actual operating process at present. In the later research, we will pay more attention to the general phenomenon of flow in the draft tube and derive more general results.

Acknowledgements

The authors acknowledge that this work was financially supported by the National Natural Science Foundation, China (Grant No. 52079118), Key Research and Development Plan of Sichuan Provincial Department of Science and Technology (Grant No. 2023YFQ0021), Qinghai Province “Kunlun Talents High-end Innovation and Entrepreneurship Talent Program” Qinghai University of Science and Technology talent introduction of scientific research special grants, Central leading local (scientific and technological innovation base construction) project XZ202201YD0017C, Jiangsu South-North Water Diversion Science and Technology R&D Project (Grant No. JSNSBD202303).

[References]

- [1] Li Z G, Cheng C, Yan S N, Peng S Y, Ma B. Theoretical analysis of entropy generation at the blade interface of a tubular turbine under cooperative conditions. *Frontiers in Energy Research*, 2021; 9: 788416.
- [2] Yao D, Ma B, Li Z G. A study on pressure fluctuation characteristics of bulb tubular turbine in a plant. *China Rural Water and Hydropower*, 2019; 12: 191–196, 199. (in Chinese)
- [3] You Z. Bulb tubular power station. Beijing: China Water and Power Press, 2009; 419p. (in Chinese)
- [4] Li W X, Li Z G, Qin Z, Yan S N, Wang Z, Peng S Y. Influence of the solution pH on the design of a hydro-mechanical magneto-hydraulic sealing device. *Engineering Failure Analysis*, 2022; 135: 106091.
- [5] Zeng H J, Li Z G, Li D Y, Chen H, Li Z. Vortex distribution and energy loss in s-shaped region of pump turbine. *Frontiers in Energy Research*, 2022; 10: 904202;
- [6] Min Z, Li Q T, Li Q F, Zhang Y P, Li Z G, Deng Y X. The analysis of the flow characteristic of draft tube based on cavitation flow of bulb turbine. *China Rural Water and Hydropower*, 2016; 1: 152–157. (in Chinese)
- [7] Lu C, Chen L, Yao D. The test research for cavitation performance of bulb turbine under off-cam conditions. *Mechanical & Electrical Technique of Hydropower Station*, 2015; 38(6): 4–6, 17, 71.
- [8] Peng S Y, Li Z G, Li X R, Chai X, Liu D Y, Zhao Y Z, et al. Flow analysis of tubular turbine draft tube based on vortex analysis. *Engineering Journal of Wuhan University*, 2020; 53(8): 679–685. (in Chinese)
- [9] Kim S J, Suh J W, Choi Y S, Park J W, Park N H, Kim J H. Inter-blade vortex and vortex rope characteristics of a pump-turbine in turbine mode under low flow rate conditions. *Water*, 2019; 11(12): 2554.
- [10] Ji B, Wang J, Luo X, Miyagawa K, Xiao L Z, Long X, et al. Numerical simulation of cavitation surge and vortical flows in a diffuser with swirling flow. *Journal of Mechanical Science and Technology*, 2016; 30(6): 2507–2514.
- [11] Podnar A, Hočevár M, Novak L, Novak L, Dular M. Analysis of bulb turbine hydrofoil cavitation. *Applied Sciences*, 2021; 11(6): 2639.
- [12] Huang R F, Ji B, Luo X W, Zhai Z H, Zhou J J. Numerical investigation of cavitation-vortex interaction in a mixed-flow waterjet pump. *Journal of Mechanical Science and Technology*, 2015; 29(9): 3707–3716.
- [13] Sun L, Guo P, Luo X. Numerical investigation on inter-blade cavitation vortex in a Francis turbine. *Renewable Energy*, 2020; 158: 64–74.
- [14] Sun L, Guo P, Luo X. Visualization investigation into processing vortex rope in Francis turbine draft tube based on several vortex identification criterions. *Chinese Journal of Hydrodynamics*, 2019; 34(6): 779–787. (in Chinese)
- [15] Li D Y, Song Y C, Lin S, Wang H J, Qin Y L, Wei X Z. Effect mechanism of cavitation on the hump characteristic of a pump-turbine. *Renewable Energy*, 2021; 167: 369–383.
- [16] Lu J. Investigation on the unsteady dynamic characteristics and its mechanism induced by cavitation in a centrifugal pump. PhD dissertation. Zhenjiang: Jiangsu University, 2017. (in Chinese)
- [17] Zhang D, Zhang Q, Shi W. Basic theory and application of pump design CFD simulation. Beijing: China Machine Press, 2015. (in Chinese)
- [18] Li Z G, Li W X, Wang Q F, Xiang R, Cheng J, Han W, et al. Effects of medium fluid cavitation on fluctuation characteristics of magnetic fluid seal interface in agricultural centrifugal pump. *Int J Agric & Biol Eng*, 2021; 14(6): 85–92.
- [19] Li Z G. The research of combination relationship and performance of bulb tubular turbine. PhD dissertation. Lanzhou: Lanzhou University of Technology, 2014; 187p. (in Chinese)
- [20] Li W X, Li Z G, Wang Z Y, Wu F, Xu L C, Peng S Y. Turbulence intensity characteristics of a magneto liquid seal interface in a liquid environment. *Coatings*, 2021; 11(11): 1333.
- [21] Ruan H, Liao W L, Luo X Q, Zhao Y P, Qin H Z, Yang Z J. Effects of low pressure meridional position on cavitation performance for high-head pump-turbine. *Transactions of the CSAE*, 2016; 32(16): 73–81. (in Chinese)
- [22] Cheng C, Li Z G, He F B, Wu S Y, Zeng C C, Zhang K, et al. Influence of Solid-Liquid Two-Phase Flow on Cavitation of Tubular Turbine Blades Under Combined Conditions. *Frontiers in Energy Research*, 2022; 10: 904201.
- [23] Zhu G J, Li K, Feng J J, Luo X Q. Effects of cavitation on pressure fluctuation of draft tube and runner vibration in a Kaplan turbine. *Transactions of the CSAE*, 2021; 37(11): 40–49. (in Chinese)
- [24] Li W X, Li Z G, Han W, Li Y B, Yan S N, Zhao Q, et al. Measured viscosity characteristics of Fe₃O₄ ferrofluid in magnetic and thermal fields. *Physics of Fluids*, 2023; 35(1): 012002.
- [25] Tong B G, Yi X Y, Zhu K Q. Vortex motion theory. Hefei: University of Science and Technology of China Press, 2009; 256p. (in Chinese)